Experiments in Fluids 21 (1996) 401–409

An experimental study of supersonic microjets

S. D. Scroggs, G. S. Settles

Abstract Miniature axisymmetric supersonic nozzles were produced with exit Mach numbers ranging from 1.0 to 2.8 by forming Pyrex® capillary tubing of 0.6 and 1.2 mm inside diameter into converging-diverging channels. The nozzle contours were measured and were found to compare favorably to ideal solutions given by the axisymmetric method of characteristics. In addition, the surfaces of these nozzles were quite smooth, providing featureless flows at perfect expansion. Schlieren visualization and pitot pressure measurements of the resulting microjets were compared to the literature available for jets produced by larger-scale nozzles. A postponed transition to turbulence is noted in these microjets due to their low Reynolds number. The pitot pressure on centerline is nearly uniform at perfect expansion over core lengths up to 12 nozzle exit diameters. Supersonic microjet nozzles thus provide a more effective small-scale high-pressure gas delivery device than do sonic nozzles of comparable scale at equivalent mass flow rates. Supersonic microjets may therefore have several industrial applications.

List of symbols

δ^*	boundary layer displacement thickness, mm
d	diameter of nozzle exit, mm
L	length of nozzle diverging section, mm
L_c	inviscid core length, mm
L_s	supersonic region length, mm
M_c	convective Mach number
M_e	exit Mach number
P_b	backpressure at nozzle exit, (equal to ambient pressure in this experiment)
P_e	exit pressure of the supersonic jet
P_{be}	exit pressure ratio (P_b/P_e)
P_p	impingement pressure (pitot pressure)
P_0	stagnation pressure supplied to nozzle
P_N	overall pressure ratio (P_0/P_b)
r	radial dimension (cylindrical coordinate system), mm
r_0	radius of throat, mm
Re_d	Reynolds number, based on nozzle exit diameter
V_e	exit velocity, m/s
x	axial dimension (cylindrical coordinate system), mm

Received: 26 September 1995/Accepted: 10 April 1996

S. D. Scroggs, G. S. Settles
Gas Dynamics Lab
Mechanical Engineering Department
The Pennsylvania State University
University Park, PA 16802, USA

Correspondence to: G. S. Settles

This research was sponsored by National Science Foundation Grant DMI 9400119, as part of a study of the assist-gas dynamics of laser cutting.

1 Introduction

Many industrial processes that use air jets to deliver pressure to a workpiece use simple sonic nozzles, having a minimum cross-sectional area at the nozzle exit. A stagnation pressure of about 2 atmospheres or more produces an underexpanded supersonic jet exiting from such nozzles. The axial pitot pressure distributions delivered by these jets contain significant variations within the first few nozzle diameters along the jet axis. The inviscid core of the supersonic jet dissipates and the resulting subsonic flow also decays rapidly. Consequently, two restrictions are imposed by the choice of such a nozzle. First, the exit must be very close to the workpiece to utilize the maximum impact pressure available (i.e., within 1 or 2 nozzle diameters). Second, the complex nature of the axial pressure distribution demands that the standoff distance between nozzle and workpiece be held to a close tolerance to maintain a uniform pressure upon the workpiece. These drawbacks can limit the processes in question, and can create significant quality control issues.

An alternative to the sonic nozzle design is the application of converging-diverging (Laval) nozzles that can create uniform supersonic jets with desirable flowfield properties. One such property is a highly uniform and stable pitot pressure distribution that extends many nozzle diameters downstream along the centerline of the jet. Of course, supersonic jets may present some significant drawbacks as well. High mass flow rate and high noise levels accompany the application of jets of even moderate size. The miniature nozzles described in this study have avoided these problems by virtue of their small scale. Nozzles of exit diameters on the order of 1 mm are found to produce characteristic supersonic jets with low mass flow rates and low noise levels.

In thus reducing the scale of supersonic nozzles, some differences in the resulting jets can be anticipated when compared to larger-scale supersonic jet data such as those of Adamson and Nicholls (1959), Donaldson and Snedeker (1971), Hu and McLaughin (1990) and Zapryagaev and

Solotchin (1991). The Reynolds numbers, Re_d, of the microjets range from 40000 to 400000, which are several orders of magnitude below that of larger-scale jets. These low Reynolds numbers can be expected to affect the transition to turbulence and associated decay of the microjets. It is also likely that the boundary layer on the microjet nozzles walls may play a proportionally greater role than in their larger counterparts. These influences are assessed by flow visualization and pitot pressure measurements, and are then compared to the case of sonic nozzles and larger-scale supersonic nozzles.

2
Experimental procedure

2.1
Nozzle fabrication

Fabrication of small nozzles to obtain an approximation of the contour given by the axisymmetric method of characteristics, as discussed in John (1984), must be accomplished in a manner that will minimize the number and size of imperfections on the nozzle wall and exit lip. Such roughness will generate disturbances in the flow, an example of which is found in the early experiments on supersonic nozzle flow by Prandtl (1952). These flaws can create non-axisymmetric structures along the free shear layer, negatively influencing the resulting jet.

A unique approach to the limitations imposed by scale and the desire to produce a smooth nozzle contour is the use of thick-walled Pyrex® capillary tubing drawn under heat and tension. The workability of glass when heated lends itself to forming the desired nozzle geometry in a controlled manner, and creates no manufactured imperfections on inner surfaces, since the process is non-abrasive. The tubing is weighted at one end an the opposite end is positioned vertically in a rotating mount. A narrow propane flame heats the exposed section of tubing as it rotates to promote even heating. The tubing begins to "neck down" when it reaches its working-point temperature, contracting to produce a throat with symmetrical converging and diverging sections. Dimensional control is obtained by a combination of three factors: 1) the size of the region heated, 2) the temperature to which it is raised and 3) the weight used on the free end of the tubing. Shorter nozzles are obtained with moderate heating of a very narrow region. Control of the heating rate is critical and can be accomplished by observing that the working temperature is approached as the heated tubing begins to glow, adding a faint orange color to the blue propane flame. Best results are obtained by fixing the weight and manipulating the first two parameters. Nozzle throat dimensions can be predicted by relating a given throat dimension to the corresponding elongation for in-process control.

Measurements using bore gauges are made to determine the throat dimension, area ratio and contour of the diverging section for each completed nozzle. An axisymmetric method of characteristics computer program, developed by Carroll et al. (1986), generates the ideal contour from knowledge of the throat diameter and radius of curvature. Good agreement between this solution and the actual contour produced by the fabrication method can be approached with practice. A typical plot illustrating this agreement is shown in Fig. 1.

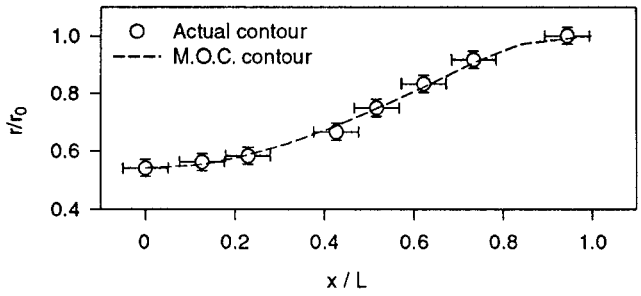

Fig. 1. Comparison of actual and method-of-characteristics nozzle contours ($r_0 = 0.6$ mm, $M_e = 2.6$, $L = 9$ mm)

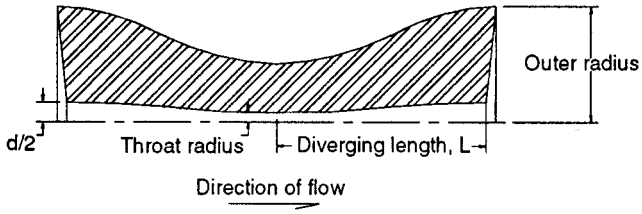

Fig. 2. Cross-sectional sketch of nozzle geometry

After forming, the glass tubing is cut to the length indicated by the characteristics code. The outside diameter of the tubing is 6 mm in the case of the 1.2 mm I.D. tubing, and 5 mm for the 0.6 mm I.D. tubing used here. A cut is made by a controlled fracture resulting in a relatively large flat "base" surrounding the nozzle exit. The nozzle exit plane is often slightly depressed from the plane of the outer diameter of the tubing, as illustrated in Fig. 2. Due to this intrinsic concave shape, the edge seen in Schlieren images of the nozzles is not the actual nozzle exit. A vertical line denotes the nozzle exit in images shown later.

The present series of nozzles range in exit Mach number from 1.0 to 2.8. The sonic nozzles were simply made from straight tubing, whereas the supersonic nozzles were fabricated as described above. The maximum attainable exit Mach number in this study was $M_e = 2.8$, dictated by the maximum area ratio that could be formed while still providing a wall thickness sufficient to contain the required stagnation pressure. Nozzles of each exit diameter were grouped by similar exit Mach number to form a test group for analyzing Reynolds number effects. Table 1 gives the measured and calculated flow parameters of the resulting test matrix. The tolerances for the data of Table 1 are as follows; diameter ± 0.03 mm, velocity $\pm 5\%$, $Re_d \pm 7\%$. In subsequent plotted data the symbol size is representative of the size of the estimated experimental uncertainty.

2.2
Experimental apparatus

The nozzles were mounted in an aluminum fixture manufactured to adapt the glass nozzle through an O-ring seal to a standard pressure fitting. This fitting, connected to 6.4 mm tubing, delivers compressed air from bottles through a 0–5000 kPa regulator. A 0–7000 kPa (accuracy ± 7 kPa) Heise gage was placed in the supply line to indicate stagnation pres-

Table 1. Supersonic microjet flow parameters

M_e	d [mm]	V_c [m/s]	Re_d
1.0	1.2	315	40000
1.0	0.6	315	20000
1.5	1.2	442	105000
1.7	0.6	467	65000
1.9	1.2	500	180000
1.9	0.6	500	90000
2.0	1.2	514	210000
2.0	0.6	514	105000
2.2	1.2	542	288000
2.2	0.6	542	144000
2.6	1.2	576	454000
2.8	0.6	604	353000

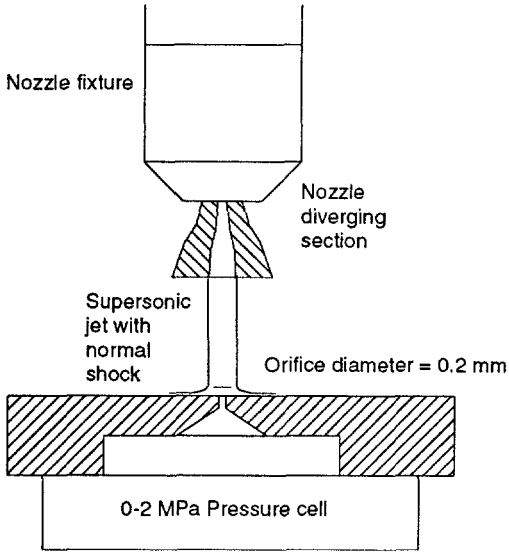

Fig. 3. Experimental arrangement

sures. Corrections were made to the data to account for frictional losses in the supply tubing based on measured pressure differential for the given flowrate by conducting tests for each nozzle size. The nozzle and fixture assembly were mounted on a dual axis micrometer drive to facilitate alignment.

The flow visualization was accomplished with a Töpler schlieren optical system, described for example in Merzkirch (1987), with 15 cm diameter field lenses of 76 cm focal length. Illumination is provided by either a halogen lamp or a microsecond-range strobed xenon arc lamp. A graded filter was used as a cutoff to avoid diffraction-based distortions. Images were recorded on S-VHS video tape using a CCD video camera. The effective video exposure time of 1/30 s provides images only of the steady-flow structures under the continuous illumination. Images are then digitized using a 16 bit, 752 × 480 pixel, PC based image processor and associated software. Halftone printing is accomplished on a Laser Jet printer.

Pitot pressures are measured by impinging the jet upon a flat surface containing a 0.2 mm diameter orifice fabricated for the purpose, as shown in Fig. 3. This plate is sealed to a 0–2000 kPa Validyne absolute pressure transducer with an accuracy of ±5 kPa. The assembly is then mounted on a computer-positioned precision X–Y table fitted with linear variable differential transducers (LVDT) to provide position indication with an accuracy of ±0.05 mm. The pressure transducer and LVDT output are recorded simultaneously on a Nicolet 430 two-channel digital oscilloscope. Sufficient data were recorded to provide a minimum of 30 data points across each nozzle exit diameter.

3
Results and discussion

Flow visualization imagery and pitot pressure surveys were analyzed to determine the effects of nozzle scale, exit pressure ratio, Mach number and Reynolds number on the resulting microjets. Variation of these parameters creates changes in the dominant features within the microjets as well as in the mixing of the microjet and the surrounding ambient gas. Where appropriate, the data were also compared to those of larger-scale jets.

3.1
Influence of nozzle geometry and scale

The size, shape and exit lip roughness of the present microjet nozzles are principal factors influencing the resulting flows, as discussed by researchers such as Donaldson and Gray (1966), Sherman et al. (1976) and Novopashin and Perepelkin (1992). They are therefore important factors to examine when attempting to maximize the pressure delivered by such a jet.

The presence of a boundary layer on the nozzle wall lowers the resulting exit Mach number compared to the inviscid prediction based on area ratio alone. An experimental measurement of the boundary layer displacement thickness was made and was compared to a theoretical estimate. This procedure is similar to that of correcting a supersonic nozzle contour for boundary layer displacement. Schlieren visualization allows the stagnation pressure at the perfectly expanded condition to be determined. This and the ambient pressure then provide a good estimate of the exit Mach number of the nozzle from isentropic flow theory. The compressible boundary layer displacement thickness, δ^*, for the case of a 0.6 mm exit diameter Mach 2.0 nozzle is thus determined to be $\delta = 0.038$ mm (i.e., 24% of the nozzle exit area). A calculation of a laminar flat plate boundary layer using the Van Driest compressibility correction yields $\delta^* = 0.042$ mm (or 26% displacement area). This compares very well with the experimental value, given the level of approximation. Both estimates constitute a larger proportion of the nozzle exit area than for larger-scale supersonic nozzles having turbulent boundary layers.

This indicates that there is a limit to how much smaller these microjet nozzles can be made while still allowing the presence of an inviscid supersonic core. The question of minimum scale has been experimentally investigated by Jindra (1970) for highly underexpanded jets ($P_N = 100$) from 2-D supersonic nozzles. Jindra determined that throat dimensions below 0.35 mm produced flows that could no longer be adequately predicted by inviscid compressible flow theory. Throat dimensions for the present microjet nozzles approach this value but are operated at a significantly lower overall pressure

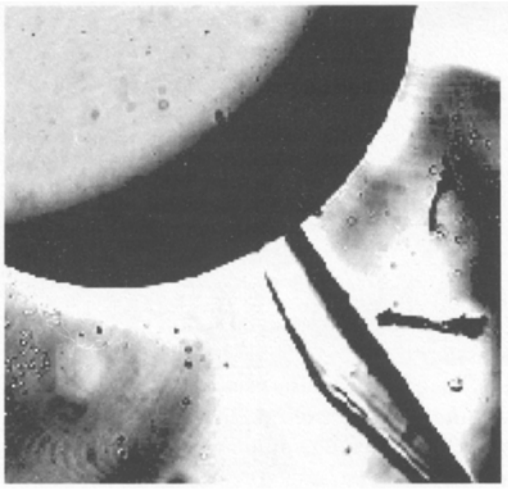

Fig. 4. Micrograph of 1.2 mm diameter nozzle with a flaw

ratio. In any case, the significant laminar boundary layer displacement thickness in microjet nozzles makes the distinction between conical and true method of characteristics nozzles take on secondary importance.

As mentioned previously, flaws at the nozzle exit are principal contributors to disturbances in the flow. Novopashin and Perepelkin (1988 and 1992) studied transition in highly underexpanded, low Reynolds number supersonic free jets ($P_N \geqslant 100$). They deduced that a surface roughness (that is, the ratio of flaw width to nozzle diameter) of less than 0.001 is required to prevent the flaw from distorting the axial symmetry of the jet, and thereby participating in the transition process. The micrograph of Fig. 4 shows a nozzle exit flaw of roughness 0.07. Flaw sizes with roughness up to 0.01 are present on all the nozzles used in this study, although an extensive survey detailing the flaws was not carried out. Likewise the role of the overall pressure ratio in the preservation of axial symmetry was not specifically investigated, however it should be noted that overall pressure ratios are much lower in the present study (typically $P_N \leqslant 50$) than in the Novopashin study. Therefore it is reasonable to conclude that nozzle exit flaws, although not always apparent in the flow visualization, participate in transition for these microjet nozzles to some extent.

3.2 Flowfield description

The flowfield of the supersonic microjets can be characterized by three distinct regions, in the same manner as are supersonic free jets of larger scale. These regions are illustrated in Fig. 5. The core region of the jet is that region where viscous effects are negligible, allowing a uniform maximum velocity and therefore uniform pitot pressure. The supersonic region, though viscous, remains above sonic speed, surrounds the core and can be characterized by the supersonic length, L_S. The change in index of refraction along the boundaries of this region allows an approximation of this length to be obtained by the schileren technique. A conical region is indicated by the change in refractive index along the boundaries of the supersonic region. This is most apparent in off-pressure conditions when wave features indicate the successively decreasing diameter of shock cells with increasing axial distance. The apex of this conical region denotes the supersonic length, L_S. Because there is some subjectivity in determining L_S by inspection of schlieren images, the accuracy of the results is estimated to be no better than $\pm 10\%$. The third region in Fig. 5 is the subsonic mixing region, which appears roughly cylindrical in laminar flow. The region then changes to a conical shape of a given spreading angle after the onset of turbulence. This cylindrical-conical shape of the subsonic mixing region is unique to low Reynolds number supersonic jets, due to their laminar exit conditions. At positions beyond L_S the velocity profile is subsonic and later becomes fully developed, as indicated in Fig. 5.

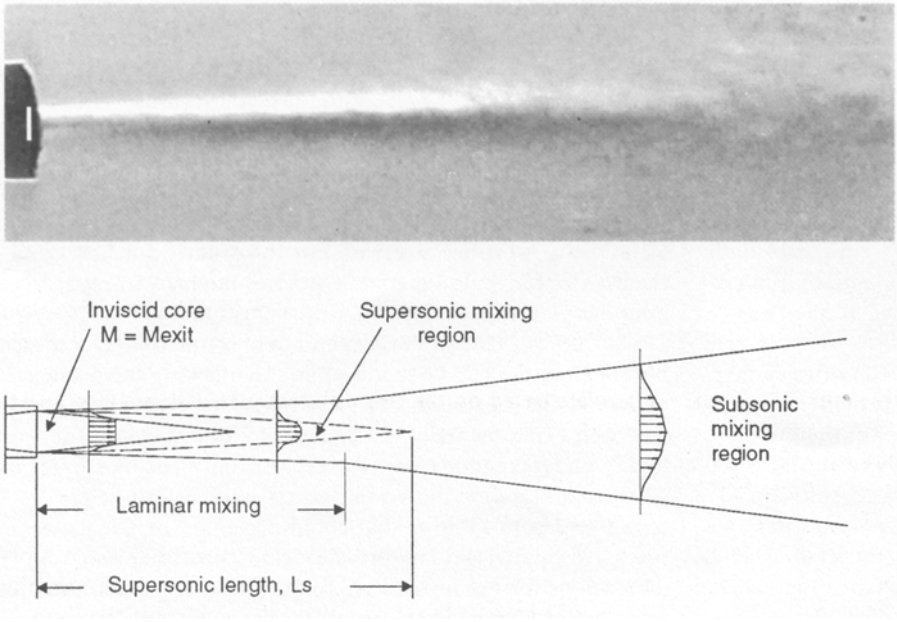

Fig. 5. Three regions of a supersonic microjet, showing approximate velocity profiles

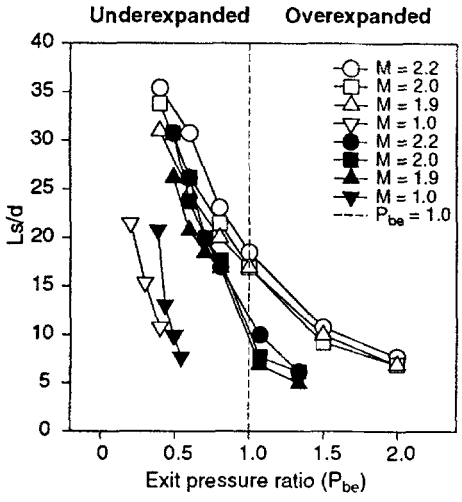

Fig. 6. Supersonic length for test nozzles; open symbols represent 0.6 mm diameter microjets, closed symbols represent 1.2 mm diameter microjets

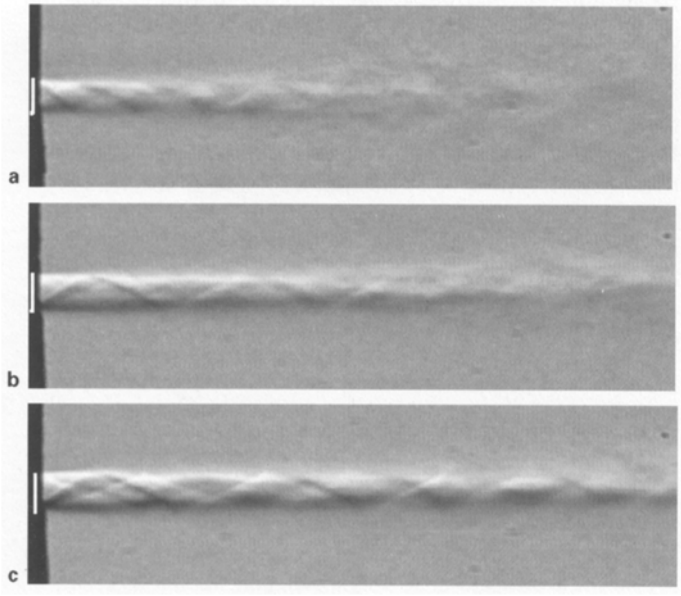

Fig. 7. Schlieren images of a Mach 2.2 supersonic jet of 0.6 mm exit diameter for **a** $P_{be}=2.0$, **b** $P_{be}=1.0$, **c** $P_{be}=0.8$

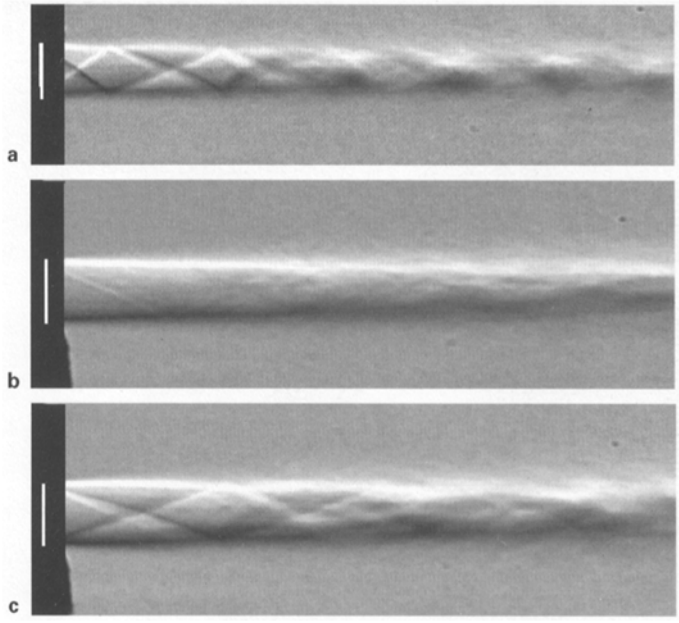

Fig. 8. Schlieren images of a Mach 2.2 supersonic jet of 1.2 mm diameter for **a** $P_{be}=2.0$, **b** $P_{be}=1.0$, **c** $P_{be}=0.8$

3.3
Jet structure versus pressure ratio

The structure of the microjets and the changes that occur through the different conditions of overexpanded, perfectly-expanded and underexpanded operation are similar for both nozzle exit diameters tested. The sonic nozzles operate in the underexpanded region for $P_{be} \leqslant 0.528$ and are subsonic above this value. Structures in underexpanded jets are similar for equal exit pressure ratio, regardless of the nozzle exit Mach number. The wave structures observed in these microjets behave in the manner predicted by classic inviscid theory, and will not be recounted here.

As seen in Fig. 6, the supersonic length grows at a slowly increasing rate with rising stagnation pressure (i.e., P_{be} decreasing) in the overexpanded condition. As expected, the flow becomes more uniform with features decreasing in strength as the exit pressure ratio nears unity.

In the perfectly-expanded condition, ($P_{be}=1$), the flow is ideally featureless and uniform since there is no pressure mismatch. The flow in the surrounding shear layer is clearly laminar as it exits the nozzle, and continues so for nearly the entire supersonic length of the present microjets.

For all underexpanded jets, the length of the supersonic region grows rapidly with increasing stagnation pressure. The maximum diameter of the shock cells increases slightly as exit pressure ratio is lowered. When the exit pressure ratio is lowered below approximately $0.35 \pm (0.05)$ for these microjets, the reflected compressions form a normal shock, or Mach disc, terminating the first shock cell. Jets containing a Mach disc in this study are termed "highly underexpanded".

Figures 7 and 8 show a series of schlieren images of Mach 2.2 microjet nozzles of 0.6 and 1.2 mm exit diameters at the over-, perfectly- and underexpanded operating conditions. A small surface flaw in the lip of both these nozzles imparts a weak wave that can be seen to propagate through the supersonic region in the perfectly expanded cases, Figs. 7b and 8b. There is no obvious difference in the structure or behavior of the microjets based on the two different nozzle diameters, apart from the location of shear layer transition.

3.4
Supersonic length and transition

The present schlieren images provide strong qualitative information as to where transition begins. By closely examining the video footage, identification of the mode of transition, the

approximate point of origin of the disturbance and a qualitative estimate of the turbulence level in the flowfield as a whole was accomplished.

Two modes of microjet transition were noted. The first is the classical shear layer instability that grows with length along the free jet mixing layer. This transitional zone is characterized by gradual radial development with axial distance. It is initially weakly visible, but gathers strength gradually along the length of the jet. The rate of growth of this type of transitional disturbance is at a minimum for perfectly-expanded jets and increases for either overexpanded or underexpanded conditions.

The second mode of transition is dependent on exit pressure ratio, and results from an acoustic feedback-generated instability, described in detail by Sherman et al. (1976). The extent of the supersonic region affected is dependent upon the exit pressure ratio, p_{be}, and can be up to 30% of the supersonic length. Acoustic waves are visible in the schlieren photos, originating in the region of the instability. No effort was made to analyze this "flapping" instability further, or to conduct extensive acoustic surveys such as those reported in Donaldson and Gray (1966), Hu and McLaughin (1990) and Morrison and McLaughin (1980).

The occurrence and mode of the transition are next described for the different conditions of supersonic nozzle operation. In the overexpanded condition the Reynolds number of a microjet is at its lowest, but the features unique to the overexpanded flow initiate disturbances that promote transition. Both modes of transition mentioned above are present in overexpanded operation. The interaction between the conical oblique shock present at the nozzle exit and the laminar boundary layer formed on the nozzle wall appears to trigger immediate transition in the laminar free shear layer at the exit of the nozzle. For all cases this disturbance is not of sufficient magnitude to immediately disrupt the supersonic region. As P_{be} approaches unity, the extent of the shear layer transition decreases throughout the supersonic length until it is minimized in the perfectly expanded condition. The acoustic feedback instability leads to transitional behavior of the second kind and marks the position, at approximately 85% of the supersonic length, where the subsonic jet region begins to spread rapidly. The entire flow is disrupted downstream of the "flapping" instability and the visible turbulent mixing is stronger than in any shear layer disturbances mentioned earlier. As P_{be} is reduced towards unity, the location of the onset of the subsonic mixing region moves downstream away from the nozzle exit.

A perfectly expanded microjet exits the nozzle in parallel laminar supersonic flow with no discernible compression or expansion waves. Under high magnification the "flapping" mode of transition can still be seen to occur at approximately 95% of the supersonic length. The subsonic region downstream of this instability is turbulent, with the apex of the roughly conical spreading angle originating at this point. Flow visualization shows that this transition occurs at a slightly earlier x/d location in the 1.2 mm exit diameter microjets, than at 0.6 mm exit diameter, which is thought to be a Reynolds number effect.

In underexpanded operation, the transition of the shear layer appears to begin at the maximum diameter of the first shock cell, where the expansion fan interacts with the free

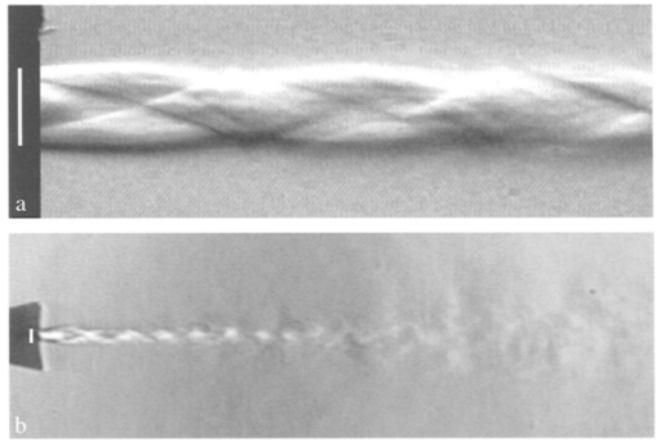

Fig. 9. Images of underexpanded $M_e = 2.0$ jets **a** high magnification showing shear layer transition under **a** strobed illumination at $P_{be} = 0.6$ and **b** constant illumination showing far field at $P_{be} = 0.4$

laminar shear layer (Fig. 9a). This interaction becomes more severe as the jet is increasingly underexpanded, and the strength of the transitional disturbances initiated at this point grows more pronounced. However, the rate of radial growth of these disturbances is not noticeably altered. This may be a compressibility effect due to high convective Mach number ($M_c = 0.8$ estimated for a Mach 2.0 microjet) as described in Fourgette et al. (1991). As the jet becomes highly underexpanded and the Mach disc appears, there is no further noticeable effect upon shear layer transition. The flapping instability is still observed in the final 15% of the supersonic regions of moderately underexpanded and highly underexpanded microjets. It is at this location that the rate of radial growth of the subsonic region increases, as seen in Fig. 9.

3.5
Reynolds number and Mach number dependence

Overall, it can be stated that transition in the two different diameter microjets is similar in mechanism, but occurs closer to the perfectly expanded condition for the larger diameter microjet. The location of the laminar free shear layer transition is also uniformly closer to the nozzle exit for the larger diameter microjets, as expected.

Nagamatsu and Sheer (1969) conducted a review of experimental data on the supersonic length as a function of jet Mach number of perfectly expanded jets. The data they cited, along with the relationship they developed, are shown in Fig. 10. The supersonic length of the present microjets, measured from the flow visualization, correlates well with the relation of Nagamatsu and Sheer. The slope of the Mach number dependence is well matched to that determined by previous investigators. Therefore, it can be concluded that the supersonic lengths of the present microjets behave similarly to those of large-scale jets in this regard.

3.6
Pitot pressure distributions

The axial pitot pressure distributions on the centerline of the present microjets were measured. The characteristics of these pitot distributions also agree well with data in the literature for

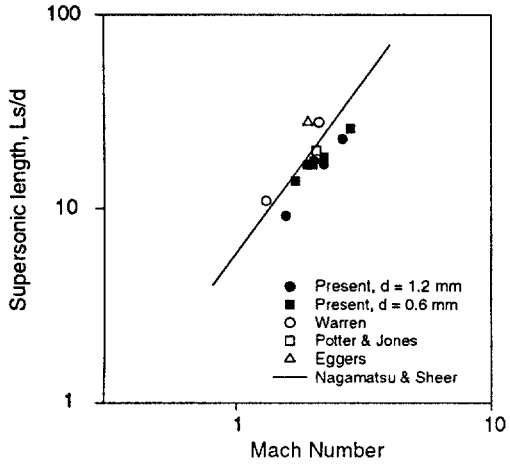

Fig. 10. Microjet non-dimensional Supersonic Length, other investigator's data and correlation of Nagamatsu and Sheer

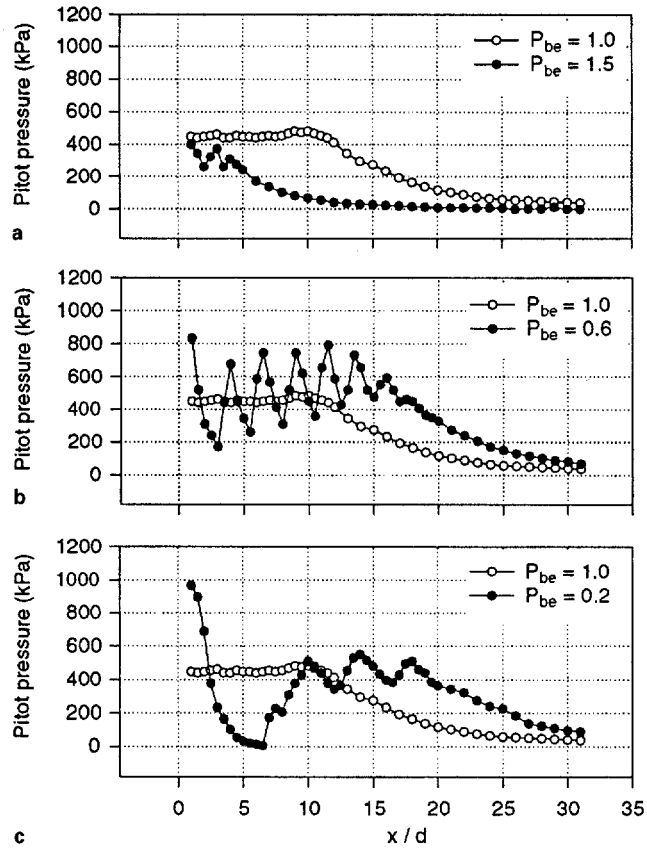

Fig. 11a–c. Axial pitot pressure distributions for Mach 2.0 jets at various Exit Pressure ratios

larger-scale jets. The pitot pressures seen in each region and under each operating condition exhibit unique characteristics. Figure 11 shows, as an example, a pitot distribution for each supersonic operating condition for a Mach 2.0 microjet of 1.2 mm diameter. The off-pressure conditions are shown as solid symbols compared to the perfectly-expanded distribution (open symbols). These results are representative of the findings for all nozzles tested.

In the overexpanded case ($P_{be}=1.5$, Fig. 11a) the low stagnation pressure produces a jet that decays rapidly. Operation in the overexpanded condition provides some practical advantage over sonic nozzles, due to its lower overall pressure variation, but is otherwise not optimal.

When the jet is near perfect expansion ($P_{be}=1.0$ in Fig. 11) the magnitude of the pitot pressure variations is minimized and the pressure remains uniformly high throughout the inviscid core. At the end of the core, the pitot pressure increases slightly before the beginning of the subsonic decay. This feature is also present in Morrison and McLaughlins' (1980) work on low Reynolds number supersonic jets. Recognizing the nearly-isentropic nature of shock waves near the sonic condition, it is reasonable to presume that this slight increase in pitot pressure is due to a wave diffusion process near the end of the inviscid core.

In Figure 11b, a moderately underexpanded case ($P_{be}=0.6$) is compared to the pitot distribution for perfect expansion. Moderate underexpansion produces the longest supersonic length for a given nozzle. The sinusoidal axial behavior of pitot pressure in this case indicates the presence of multiple shock cells.

When the highly underexpanded condition is reached ($P_{be}=0.2$, Fig. 11c) the presence of the Mach disc exacts a large penalty in jet stagnation pressure. Sonic nozzles reach this highly-underexpanded condition quickly, with P_N as low as 2.6.

Pitot pressure surveys normal to the axis of the present microjets confirm the results of the flow visualization. Figure 12 displays one such survey showing radial pitot pressure distributions taken at $x/d=1$, 6, 11, and 16 along the axis of a perfectly expanded Mach 2.0 microjet of 1.2 mm diameter. The pressure distribution has a top-hat shape in Fig. 12a and 12b which becomes roughly Gaussian in shape farther from the nozzle exit in Fig. 12c and 12d. In agreement with the flow visualization, these pitot pressure surveys indicate that the width of the microjet experiences no appreciable growth until the subsonic mixing region is reached. The sharp pressure gradients along the boundaries of the jet suggest that microjets will be sensitive to alignment in practical applications.

Taken collectively, the present pitot pressure surveys lead to several noteworthy observations. Figure 13 displays all the axial pitot profiles for perfectly expanded microjets of various exit Mach number with a single underexpanded case from a sonic nozzle (at $P_{be}=0.3$) shown for comparison. Maximum pitot pressure and core length are observed to increase with rising exit Mach number. For example, a Mach 2.6 nozzle requires a stagnation pressure 3 times that of a Mach 2.0 nozzle for perfect expansion, but only yields a 33 percent increase in pitot pressure and a 10% gain in core length. The diminishing return in pitot pressure is largely a result of the increasing loss inherent in the normal shock formed upon jet impingement on the pressure measuring surface. Comparing the perfectly expanded pitot distribution to that of the underexpanded sonic nozzle jet in Fig. 13 illustrates the practical advantages of using supersonic (Laval) nozzles. Both higher pitot pressures and less sensitivity to axial distance are seen with the Laval nozzles. Moreover, calculations for a sonic nozzle and a $M_e=2.0$ nozzle of equal exit diameter show that all the advantages of the latter can be had at about the same mass flow rate.

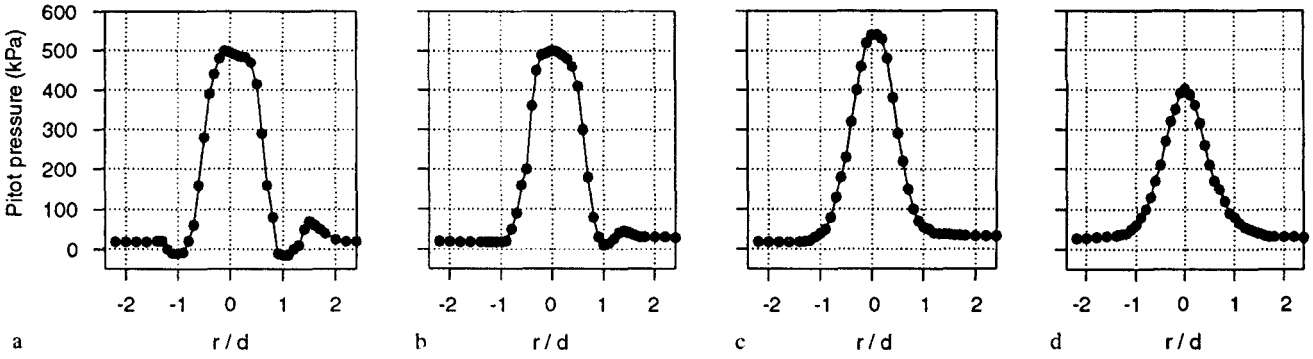

Fig. 12. Radial pitot surveys taken at axial locations **a** $x/d=1$, **b** $x/d=6$, **c** $x/d=11$, and d) $x/d=16$ describing the width and magnitude of the pitot pressure distribution in the microjet. ($M_e=2.0$, $d=1.2$ mm, $P_{be}=1.0$)

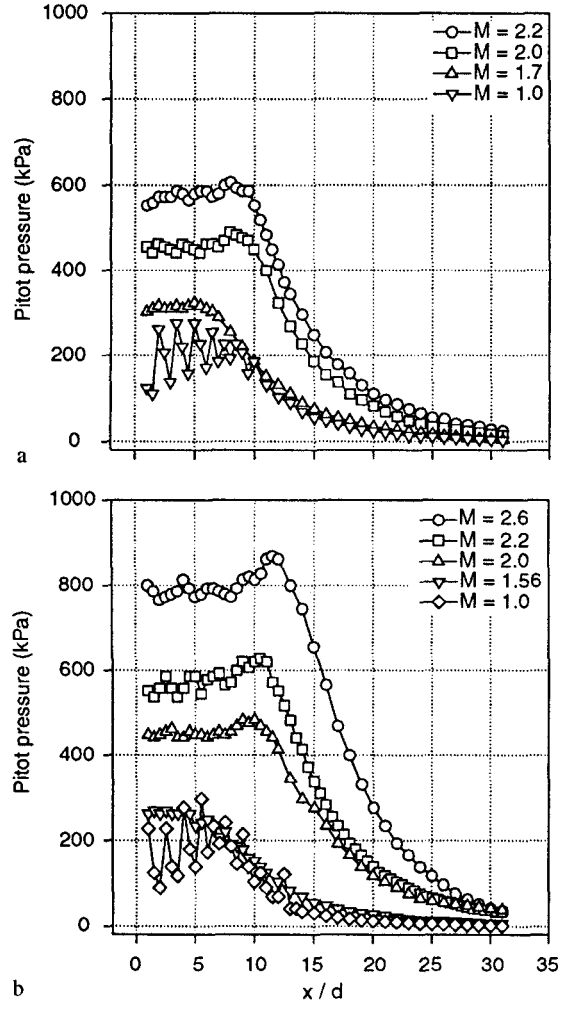

Fig. 13. Perfectly-expanded and sonic nozzle pitot profiles for **a** d = 0.6 mm, **b** 1.2 mm. Sonic nozzle distribution shown for $P_{be}=0.3$

The pitot pressure distributions for the larger-diameter microjets in Fig. 13 indicate a longer nondimensional core length than those of the smaller-diameter microjets at equal exit Mach number. The pitot orifice, however, being the same size for both nozzles was comparatively 3.5 times larger for the case of the smaller-diameter microjets. It is reasonable to assume, then, the that the relative size effect of the pitot orifice contributed to a less-accurate measure of the core length in these cases.

4 Conclusion

A unique method of fabricating small-scale supersonic nozzles capable of producing nearly perfect supesonic microjets up to Mach 2.8 has been developed. The flows issuing from these nozzles have been analyzed and compared to the literature on larger-scale supersonic jets and underexpanded jets produced by sonic nozzles of higher Reynolds numbers. A postponed transition to turbulence is the most notable effect of the reduction in scale. While viscous effects are accentuated in the nozzle wall boundary layer, the applicability of one-dimensional isentropic compressible flow theory is not yet compromised at this scale. Other aspects of supersonic free jets, such as the Reynolds number and Mach number dependence of supersonic length and core length, correlate well with experimental data in the literature for large-scale supersonic jets. The ability of perfectly-expanded supersonic microjets to project a relatively stable and uniform pitot pressure at a distance of 10 or more exit diameters was demonstrated. These results indicate that microjets offer significant potential for a variety of industrial processes.

References

Adamson T; Nicholls J (1959) On the structure of jets from highly underexpanded nozzles into still air J. Aero/space Sci. Jan 16–24

Carroll BF; Dutton JC; Addy AL (1986) NOZCS2: A computer program for the design of continuous slope supersonic Nozzles. University of Illinois at Urbana-Champaign, Report No. UILU ENG 86–4007

Donaldson C; Gray KE (1966) Theoretical and experimental investigation of the compressible free mixing of two dissimilar gases. AIAA J 4: 2019–2028

Donaldson C; Snedeker R (1971) A study of free jet impingement. J Fluid Mech 45: 281–319

Fourgette DC; Mungal MG; Dibble RW (1991) Time evolution of the shear layer of a supersonic axisymmetric jet AIAA J 29: 1123–1130

Hu T; McLaughin D (1990) Flow and acoustic properties of low Reynolds number underexpanded supersonic jets. J of Sound and Vibration 141: 485–505

Jindra KJ (1970) Geometric effects on the performance characteristics of very small nozzles. Masters Thesis, Air Force Inst. of Tech., Wright-Patterson AFB, Ohio School of Engineering, Dec.
John JEA (1984) Gas dynamics. 2 ed., New York: Prentice Hall
Merzkirch W (1987) Flow visualization, 2 ed. Orlando: Academic Press
Morrison GL; McLaughlin DK (1980) Instability process in low Reynolds number supersonic jets. AIAA J 18: 793–800
Novopashin SA; Perepelkin AL (1988) Axial symmetry loss of a preturbulent jet. Phys Lett 135: 290–293
Novopashin SA; Perepelkin AL (1992) Transition to turbulence in a supersonic jet. Russian J Eng Thermophys 2: 51–61
Nagamatsu HT; Sheer RE (1969) Supersonic jet noise theory and experiments. NASA SP-207
Prandtl L (1952) The essentials of fluid dynamics. Glasgow: Blackie & Son
Sherman PM; Glass DR; Duleep KG (1976) Jet flowfield during screech. Appl. Scient. Res. 32: 283–303
Zapryagaev VI; Solotchin AV (1991) Three-dimensional structure of flow in a supersonic underexpanded Jet. J Appl Mech Tech Phys 32: 503–507